water

MDPI

Article

Characterization of Karst Conduit Network Using Long-Distance Tracer Test in Lijiang, Southwestern China

Jihong Qi, Mo Xu *, Xinyu Cen, Lu Wang and Qiang Zhang

State Key Laboratory of Geohazard Prevention and Geoenvironment Protection, Chengdu University of Technology, Chengdu 610059, China; Joannqi@hotmail.com; (J.Q.); cenxinyukl2@163.com (X.C.); wl604890182@163.com (L.W.); zhangq@cdut.edu.cn (Q.Z.)

* Correspondence: XM@cdut.edu.cn; Tel.: +86-138-0819-9827

Received: 19 June 2018; Accepted: 12 July 2018; Published: 16 July 2018

Abstract: The Ancient City in Lijiang of southwestern China was endowed as World Cultural Heritage by UNESCO, and the karst springs located in Black Dragon Pool are its main water source. However, the springs have dried up several times in recent years, which caused serious damages to the landscape as well as the city water supply. Triggered by the dried-up event in Black Dragon Pool, a long-distance artificial tracer test up to 17 km was employed to investigate the karst conduit network distributing in the study area. Based on the tracer concentration breakthrough curves (BTCs), the hydraulic connection from the same injection point (located in a giant depression named the Jiuzi Sea) to the springs on both sides of the topography watershed was proven, and the conduit structure was discussed. According to the characteristics of BTCs and considering the low tracer concentration and tracer recovery, a conceptual structure of leaky reservoir with threshold effect above a certain groundwater level was established to interpret why the springs in Black Dragon Pool dried up several times in history, but those in the Ancient City never did. Furthermore, a method of injecting surface water into the Jiuzi Sea to raise the groundwater level up to the height of Black Dragon Pool was proposed to restore the springs. Our study provides insights into the long-distance artificial tracer test, and opens a new avenue for groundwater resource recovery of this Ancient City.

Keywords: water resource; tracer test; karst conduit structure; tracer recovery; Lijiang Ancient City

1. Introduction

Karst aquifers are complex systems with heterogeneous nature, and some special hydrogeological methods are often required to understand their spatial characteristics. Among these methods, the artificial tracer test is one effective technology that can give direct information on the hydraulic connection, paths structure and hydrogeology parameters [1–3]. More than 100 years ago, the artificial tracer technology was initially applied in the United States to identify underground connections. With the improvement of experimental conditions, linear flow velocities and other relevant parameters can be further quantified, and it is possible to interpret tracer breakthrough curves to establish a structural model of a karst aquifer [4–8].

Relevant research on the karst tracer test in China mainly concentrates on the speculation of the whole spatial structure. Based on the field test data, Yang and Zhang considered that the number of independent main peaks on the BTCs reflected the number of main conduits in the karst system [9,10], which is verified by physical experiments [7]. Some research also shows that the karst conduit flow corresponds to the BTCs with large kurtosis, reservoirs on the conduit could lead to gradual descending or steps on the falling limb of the curves [11]. The tracer test with high-precision online monitoring

technique in Maocun has obtained more accurate BTCs, revealing that there are multiple conduits in the underground karst system or there are many reservoirs on the flow path [9]. At present, the karst tracer test in China is mainly concerned about the structural inference of the whole system, while the research on the transport characteristics of the tracer in the system is relatively scarce.

Based on some parameters from tracer test, researchers paid attention to the transport characteristics of tracer and the quantitative study of the karst system. Smart argued that curves may be characterized by a few parameters, including the travel time, the time-concentration integral and the dimensionless recovery ratio [12]. According to the above parameters, a robust methodology for determining the relationships between springs was provided [4]. Research on Lurbach system reveals that the solute-transport in the karst aquifer is most likely influenced by the combination of two processes: the partition of groundwater flow into a hierarchic conduit network, and the mass transfer between mobile and immobile continuous zones within the conduit [13]. Notably, it can be explained that the rapid flow velocity and low tracer recovery rate are the characteristics of tracer test in the mildly karst aquifer, especially in long distant tracer test [14,15], but the tracer distance is often less than 10 km in previous reports.

Using a long-distance tracer test up to 17 km, this work aims to measure the network of karst conduits in Lijiang, southwestern China. Lijiang is famous for the Ancient City endowed as World Cultural Heritage by UNESCO. Triggered by the dried-up event in Black Dragon Pool, it is an important method to investigate the characteristics of the conduit structure in this karst system for solving the above problem. In this study, based on the tracer BTCs at 10 receiving points and the discussion of the flow velocity and recovery ratio, the conduit structure of karst system in the study area was deduced and the dried-up mechanism of Black dragon Pool was explained in detail. Furthermore, the experiment shows the possibility of speculating the conduit structure by artificial tracer tests within the long karst system and provides an effective way to recover water resources in this study area.

2. Materials and Methods

2.1. Study Area

Lijiang City is located in the northwest of Yunnan Province (Figure 1A), China. Over 28% of Yunnan Province exhibits the karst topography [16]. Lijiang is famous for its Ancient City built about 900 years ago [17], which is located at the foot of the Elephant Mountain composed mainly by karst rocks. The groundwater discharge involves a series of springs, which are called as “soul of the city”. Over the past century, Black Dragon Pool springs have dried up many times despite their ever large flow. The longest cutoff time even lasted for 810 days from 1984 to 1986, and the cutoff frequency has also increased from once every twenty years to once every five years since 1960 [18,19]. Therefore, the Ancient City faces serious crisis of spring drying and landscape decaying.

As shown in Figure 1C, about 70% of the study area is constituted by karstified terranes. The north part is the mountainous region rising by 2700–3500 m, and the south part is the graben basin where the Ancient City is located, with an elevation of about 2410 m. The Jinsha River flows around the area, and a minor river named the White River flows eastward to join the Jinsha River (Figure 1B). As a result of its deeply rugged topography, the White River becomes the northern boundary of the groundwater flow in the study area. The climate of this area can be classified as Plateau Monsoon Climate with an average annual precipitation of approximately 1000 mm (about 90% rainfall occurs from May to October) and an average annual temperature of 16.3 °C.

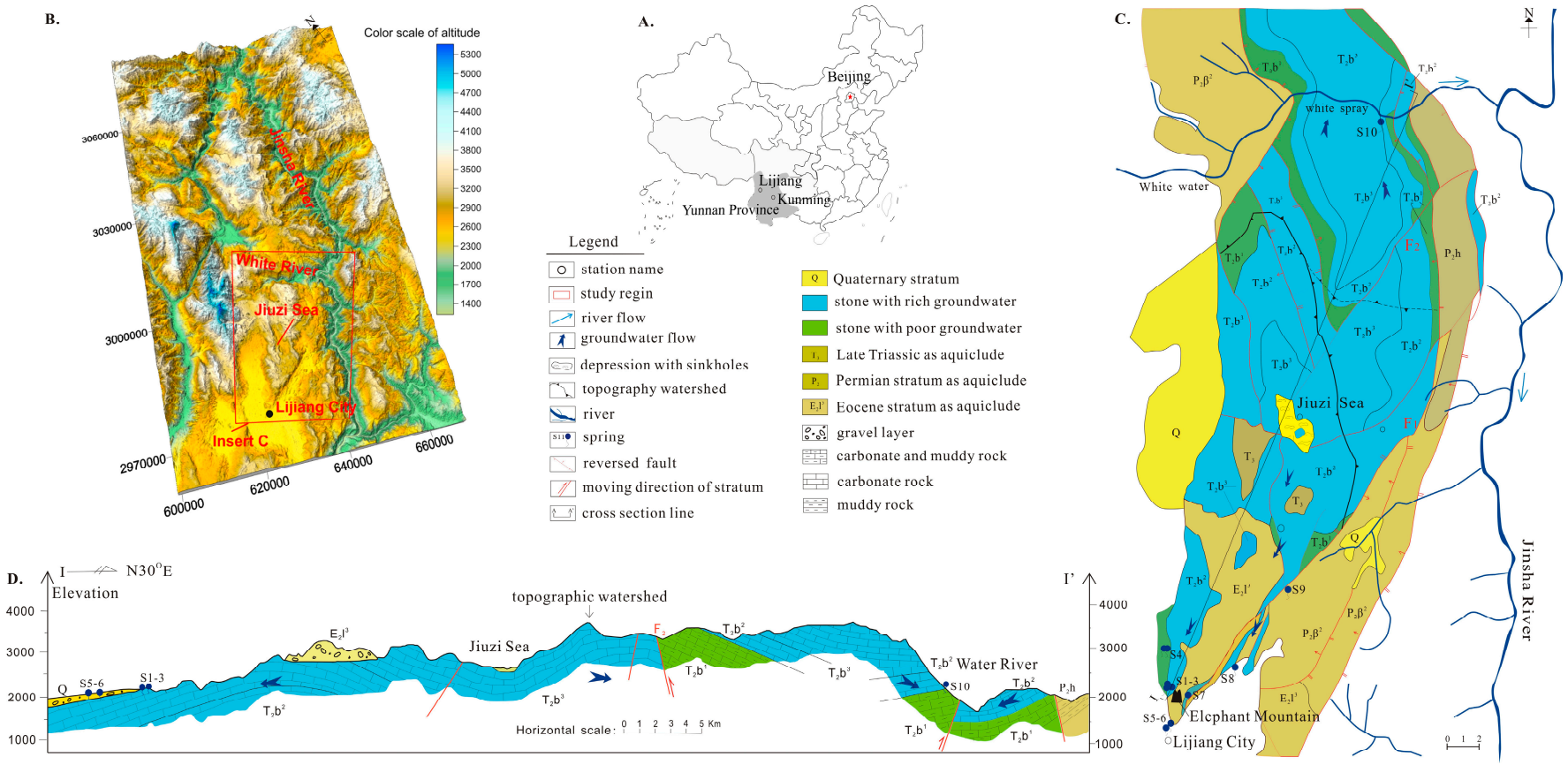

Figure 1. The location of the study area and the sketch of hydrogeological environment the location of Lijiang; (**A**) the location of Lijiang in China; (**B**) the range of the studied area; (**C**) the sketch of hydrogeological environment of the study area; and (**D**) the hydrogeological cross section of I-I′ (the cross section line is shown in (**C**)).

2.2. Geological and Hydrogeological Features of the Study Area

The geological structure and hydrogeological context of the study area are illustrated in Figure 1C,D. This area has a cone shape towards southwest. The stratum of Triassic Beiya group (T_2b^1–T_2b^3) is the main aquifer of the groundwater, covering the middle area of the mountains. The strata of T_2b^3 and T_2b^2 are composed of carbonate rocks, and T_2b^1 stratum is carbonate with muddy rocks. Permian is basalt stratum, which extends to the east of F_1. Because the basalt is an aquitard stratum, some part of groundwater discharges along F_1. Hence, it is considered as the eastern boundary of the study area. Quaternary stratum composed of muddy and sand rocks distributes over the Ancient City, and it is an aquiclude stratum, which is considered as the western and southern boundaries.

There is another important fault of F_2 which extends from a giant depression named the Jiuzi Sea to the area near the White River (Figure 1C) and cuts the topography watershed between the north boundary (the White River) and the Ancient City. The giant karst depression with several sinkholes (Figure 1C) has an area of about 8.2 km^2 and its extension length is 2840 m. The mountainous area around it has an altitude of 3000–3500 m. It is famous for the numerous natural pools in the karst depression due to blocked sinkholes. This giant and closed karst depression surrounded by high mountains has good catchment conditions, and the mountains between the White River and the Ancient City are the main supply source for the groundwater in Lijiang.

On the boundary, the karst groundwater discharges intensively as springs (Figure 1C and Table 1). All of them are recharged from rainfall, and swallow holes in the karst area can serve as the recharge paths. Three springs (S1, S2, and S3) are located in Black Dragon Pool, and they are the main water source for the Ancient City. The biggest flow rate in their history was about 1 m^3/s, but the flow rate has decreased sharply in recent years and even dried up a few times. Other springs have never dried up. Their flow rates are relatively smaller and almost keep constant during the test period, as shown in Figure 2. In the Ancient City, a few springs (S5, S6, and S7) appear at lower altitudes, whereas the altitudes of the springs along F_1 (S8 and S9) and the Clear Reservoir (S4) on the west boundary are higher than those of the springs in Black Dragon Pool. All these above-mentioned springs are located in the south to the topography watershed. In addition, there is a big spring known as S10 located in the White River, which is the main groundwater outlet of the northern part.

2.3. Methodology

The methodology was based on the artificial tracer test from November to December in 2014, as well as the long-term monitoring on a few springs and surface meteorological conditions. During the tracer test, the flow rate of all springs except for S10 was lower than 40 L/s. Before the test, we made a simple tunnel to export each spring, and installed a poling board in the tunnel. This tunnel could make the spring flow through the poling board. By comparison with the scale on the poling board, the water level could reflect the discharge (L/s); the accuracy of the discharge determination is 0.1 L/s. S10 was used for power generation, and its discharge record came from the power station. The flow rates of all springs are almost constant during the test period according to the records. Meteorological data were provided by the Royal Meteorological Institute of Lijiang City. There are three meteorological monitoring stations located in the Jiuzi Sea, Black Dragon Pool, and Clear Reservoir, respectively. November and December are the driest months of the year in Lijiang. There was no rainfall in the study area during the experiment, which ensured that the variation of the tracer concentration in each spring was only derived from the karst aquifer itself.

The selection of tracers should be based on the standard that the tracers can be measured simultaneously on site with low detection limits to get smooth and high-resolution BTCs in time [20,21]. Under this premise, KI and uranine were selected as tracers. KI powder is easily soluble in water and I^- can be utilized by organism, whose background concentration is less than 5 ppb. Uranine is used frequently for groundwater tracing in Karst area, which is environmentally compatible, allowing detection at very low concentration, but can be adsorbed by the soil and aquifer [22–25]. The tracers in

water samples were measured in laboratory by a DR6000 UV spectrometer (uranine at the maximum absorption spectrum of 512 nm with a detection limit of 0.1 ppb and KI at the maximum absorption spectrum of 570 nm with a detection limit of 50 ppb, as shown in Table 2). Before the tracer test, standard samples for every receiving spring were collected. The two tracers were added into water simultaneously, and the solution was well mixed.

The amount of tracer required depends on the properties of tracer and anticipated flow type. Field [26] reviewed 33 tracer mass estimation equations, most of which are based on experience. Worthington and Smart [27] suggested an adaptable formula for karst tracing:

$$\boldsymbol{M} = 1.95 \times 10^{-5} (\boldsymbol{LQC})^{0.95} \quad (1)$$

where $\boldsymbol{M}$ is tracer quantity, i.e., mass [kg]; $\boldsymbol{L}$ is distance [km]; $\boldsymbol{Q}$ is discharge [L/s]; and $\boldsymbol{C}$ is target peak concentration [μg/L]. The estimated total flow of springs in the study area can be obtained from Equation (2) [28].

$$\boldsymbol{Q} = \boldsymbol{\alpha} \cdot \boldsymbol{P} \cdot \boldsymbol{F} \quad (2)$$

where $\boldsymbol{Q}$ is the groundwater discharge from rainfall [L/s], $\boldsymbol{\alpha}$ is the infiltration coefficient, $\boldsymbol{P}$ is the annual average rainfall (1000 mm) from the Meteorological Monitoring Station located in the Jiuzi Sea, and $\boldsymbol{F}$ is the catchment area [km^2]. $\boldsymbol{\alpha}$ is determined as 0.4 during the test period considering the topography, the karst development degree and the climate [29,30], and the catchment area $\boldsymbol{F}$ is determined as 33.7 km^2 considering the geology situation and infiltration conditions at the surface and topography. Thus, the calculated $\boldsymbol{Q}$ is 397 L/s. L is 18 km considering the max distant between the injection point and receiving springs, and target peak concentration is 40 μg/L for uranine and 5000 μg/L for KI considering the detection limit (Table 2). According to the calculated $\boldsymbol{Q}$ and considering the detection limit of the tracers, 3 kg uranine and 400 kg KI were dissolved in about 300 m^3 water, and then the solutions were injected into the sinkhole within 2 h. To ensure the tracers were injected into groundwater, about 1×10^6 m^3 water was pumped into the sinkhole for 24 h.

The most uncertain aspect of any tracing study is the schedule for sample collection [25,31]. For solution conduits, an expected average transport velocity equal to 0.02 m s^{-1} may be used as the basis for designing a sampling schedule [26]. This average transport velocity of 0.02 m s^{-1} was statistically determined by regression analyses of more than 3000 tracing tests worldwide [27]. The average velocity is rough estimate and represents a rough average velocity time. Basing on this, the sampling frequency in our tracer test is suggested in Table 3, and adjusted to ensure that initial sample collection begins prior to likely tracer breakthrough. During the tracer test, varied frequency sampling method was applied. The sampling frequency increased with time extension, from once a day to once every 2 h during the expected tracer peak period (discussed below). The highly-frequent sampling lasted until the peak pulse passed, and then the sampling frequency decreased for the next few days.

2.4. Injection Points and Receiving Springs

The springs are located on both sides of the topography watershed (Figure 1C). Ten springs were monitored continuously for about 40 days as soon as the tracers were injected. Based on their locations, these ten receiving springs can be divided into five systems (Table 1).

Table 1. Characterizations of every spring as receiving point.

Receiving Points	The Situation to the Topography Watershed	Receiving Points		Height (m)	Mean Water Volume [1] (L/s)	Lithology of Spring	Direct Distant from Injection Point (km)	Flow Fluctuation in History Especially Comparing to Datum in 1970s
		Station	Name of Receiving Point					
S1	south to the topography watershed	Black Dragon Pool	Longevity spring	2420	0.5	T_2b^2/pure limestone	16.4	The biggest volume in 1970s is 1000 L/s and dried up several times. During the tracer test period, the springs have been recovered for one year.
S2			Pearl spring	2420	33.5			
S3			Gate spring	2420	5.5			
S4		Clear Reservoir	Clear spring	2433	40.0	Quaternary/Grave	15.6	Volume reducing but never dry up in history
S5		Ancient City	White horse Pool spring	2397	14.2	T_2b^2/pure limestone	16.2	Constant and never dry up
S6			Eyes Well spring	2408	3.1			
S7			Sweet spring	2396	17.4	T_2b^2 pure limestone	15.3	
S8		Along the F_1	Lotuses spring	2421	7.0		12.9	
S9			Rock spring	2497	3.9	T_2b^3/limestone and muddy stone	9.4	
S10	north to the topography watershed	White water River	White spray spring	2015	140.3	T_2b^2/pure limestone	16.8	Never dry up but reduce in dry year

[1] The mean volume calculated in tracer test period.

Table 2. Characterizations of two tracers used in this test.

No.	Tracer Material	The Amount of Tracer (kg)	Limit of Detection (ppb)	The Maximum Absorption Spectrum (nm)	Injecting Time and Volume of Tracer Solutions	Injecting Time and Volume of Pure Water
1	Uranine	3.0	0.1	512	2 h/1200 L	24 h/(1×10^6) m^3
2	KI	400.0	50	570		

Table 3. Sampling schedule in our tracer test [1].

Time (Day)	Day 1–4	Day 5–6	Day 7–(X * + 2)	Day (X * + 2)–(X * + 5)	Day (X * + 5)–Y
Sampling interval (h)	12	6	2–4	4–6	12

[1] Modified from Käss [32]; X represents the time (day) when the tracer peak arrives. Y represents the time (day) when the concentration of tracers cannot be detected. * The time is estimated peak time using the equation: $t_p = S/v$, where S is the direct distance between the injection points and receiving springs, and v is the 0.02 m s^{-1} [25].

On the south of the watershed, there are four stations at the boundaries of the study area. Discharging from the stratum of T_2b^2, three springs (S1, S2 and S3) are located in Black Dragon Pool at the foot of the Elephant Mountain, and the altitude of these springs is 2420 m. Discharging into the Clear Reservoir, the Clear Spring (S4) appears from the Quaternary stratum to western T_2b^2 stratum, and its altitude is 2433 m, which is higher than that of Black Dragon Pool. The springs (S5, S6, and S7) in the Ancient City are lower than those in Black Dragon Pool, and all of them discharge from the stratum of T_2b^2. The other two receiving springs are S8 and S9 along F_1. S8 discharges from T_2b^2 and S9 from T_2b^3. Their altitudes are higher than that of Black Dragon Pool. On the northern part of the watershed, S10, known as the White Spray Spring, discharges into the White River at the north boundary of the study area. Its altitude is only 2015 m, which is significantly lower than that of those southern receiving springs. It has never dried up in history and its flow rate is the biggest of all receiving springs.

There is only one injection sinkhole located in the depression of the Jiuzi Sea. The stratum around the Jiuzi Sea is T_2b^2, and its altitude is 2840 m. There are a few sinkholes in this depression, and some are blocked to form pools. After investigation, we believe that this injection sinkhole is unblocked, but its scale and structure are not clear.

3. Results

3.1. BTCs of Receiving Springs at Different Locations

In this study, two different color curves are used to represent concentration fluctuations with time extension. $C(t)/C_p$ as a function of time is plotted [33,34], where $C(t)$ is the tracer concentration at a certain detecting time, and C_p is the peak concentration during the test period. The detecting time is the injection time ($t = 0$) as the reference. In Figure 2A–J, all receiving springs have different shapes and peak times (Table 4), while the peak pulse of these two tracers show similar peak ratio value, the resident time, and the interval of peak pulse.

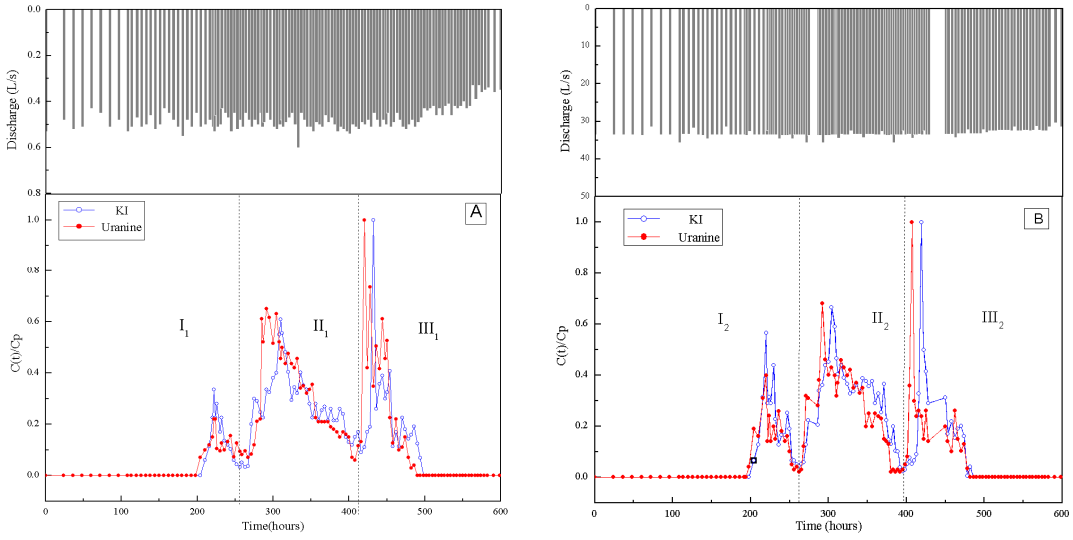

Figure 2. *Cont.*

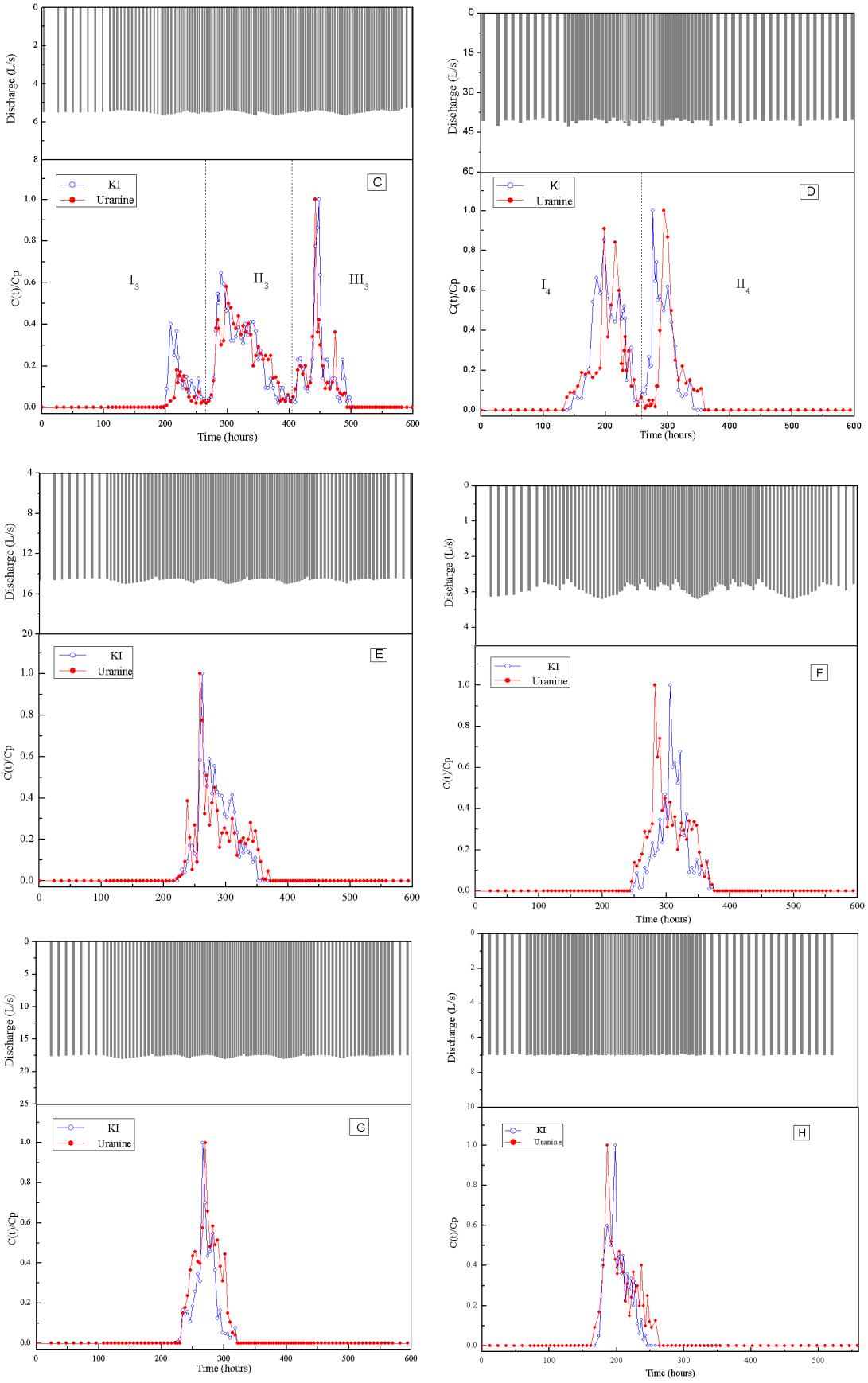

Figure 2. *Cont.*

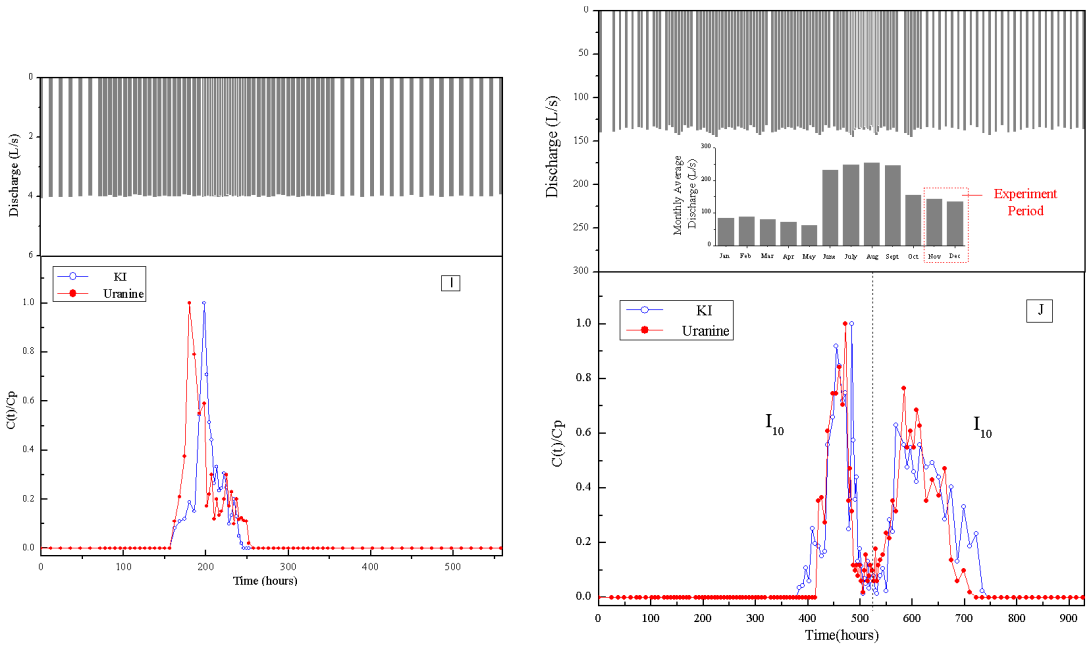

Figure 2. Breakthrough curves of tracer concentration (KI and Uranine) in every receiving point. The tratio of concentration to the maximum shown as C(t)/Cp: (**A**–**C**) S1, S2 and S3 located in Black Dragon Pool; (**D**) S4 discharging into the Clear Reservoir; (**E**–**G**) S5, S6 and S7 located in Ancient City; (**H**,**I**) S8 and S9 distributing along F1; and (**J**) S10 discharging into the White River.

3.1.1. Curves with Multi-Peaks

The BTCs of the two tracers received from the three springs of Black Dragon Pool (S1, S2, and S3) exhibit three major peaks, and the second peak is the primary one considering the long resident time, and slow decline of concentration. The time of the first detection is about 200 h for these three springs (shown in Table 4). There are two major peaks on both curves in Figure 2D for S4, and the shape of the uranine curve is very similar in I_4 and II_4 sections. The time of first detection is 198 h which is similar to the springs of Black Dragon Pool.

Two major peaks can be found on both curves in Figure 2J for S10, and the second peak is the primary one considering the long resident time, and slow decline of concentration. The White Spray Spring (S10) is the only receiving spring at the north to the Jiuzi Sea, and has different hydrogeological conditions from all other receiving points located at the south to the Jiuzi Sea. Thus, it takes much longer time receive the tracers. In fact, KI and uranine were firstly detected at the White Spray spring after the tracers were injected into the Jiuzi Sea for 384 h and 414 h, respectively. The last time for second peak is about 210 h.

3.1.2. Curves with Single Peak

There is only one major peak with weaker tailing on both curves in Figure 2E–I. Similar to III_{1-3}, there are many small fluctuations in Figure 2E. The White Horse Pool spring (S5), Three Eyes Well spring (S6) and Sweet spring (S7) are located in the Ancient City. The distance from any of the three receiving points to the Jiuzi Sea is similar to that from the springs in Black Dragon Pool to the Jiuzi Sea, but it takes more time to receive the tracers in the Ancient City than in Black Dragon Pool. The Rock and Lotuses springs are located along F_1, as shown in Figure 2I,J, tracers were first detected in the two springs, and their peak times appear earlier than all the other springs.

3.2. Tracer Recovery and Average Concentration

Estimation of tracer recovery for individual sampling stations is given by Equation (3) and total tracer recovery from all down gradient receptors may be estimated with Equation (4) [35].

$$M_{0i} = \int_0^{\infty} C_i(t)Q_i(t)dt \approx \sum_{i=1}^{m} Q_i C_i \Delta t_i M_0 = \sum_{i=1}^{n} M_{0i} \quad (3)$$

The rate of tracer recovery can be calculated by Equation (5).

$$\mathrm{R} = \frac{M_0}{M_T} = \sum_{1}^{n} Q_i C_i \Delta t_i / M_T = \sum_{1}^{n} R_i \quad (4)$$

where M_{0i} is the weight of every receptor's tracer recovery [kg], t_i is any necessary time [s], n is the number of the receptors [unitless], Q_i and C_i are spring discharge (L/s) and concentration of tracer [ppm], M_0 is total weight of tracer recovery [kg], M_T is the weight of injected tracer [kg], R_i is the ratio of tracer recovery of every receptor, and R is total ratio of tracer recovery of all receptors.

These models assume complete mixing of the tracer substance with water, negligible dispersion effects, and that the tracer mass will ultimately exit the aquifer system completely at one or more down gradient receptors as a function of time and discharge. The tracer recovery of every receiving springs is shown in Table 5. The total recovery is only 13.68% of KI, and 15.62% of uranine. It shows the very low tracer recovery during the detection period.

Before calculating the average concentration of tracer, we firstly determine the starting and ending time point of tracer receiving at each receiving spring according to Figure 2. The average concentration of the tracer calculated according to the above formula is shown in Figure 3.

$$\overline{y} = [\sum_{i=1}^{m-1}\left(\frac{Q_i + Q_{i+1}}{2}\right)(t_{i-}t_{i+1})\left(\frac{y_i + y_{i+1}}{2}\right) / \sum_{i=1}^{m-1}\left(\frac{Q_i + Q_{i+1}}{2}\right)(t_i - t_{i+1}) \quad (5)$$

where $\overline{y}$ is the chronological average of tracer concentration [ppm], Q_i is flow rate at i time point [L/s], y_i is tracer concentration at i time point [hours], m is the number of time point items [unitless], t_1 represents the time when the tracers are first detected, and t_{m-1} represents the time when the tracers cannot be detected.

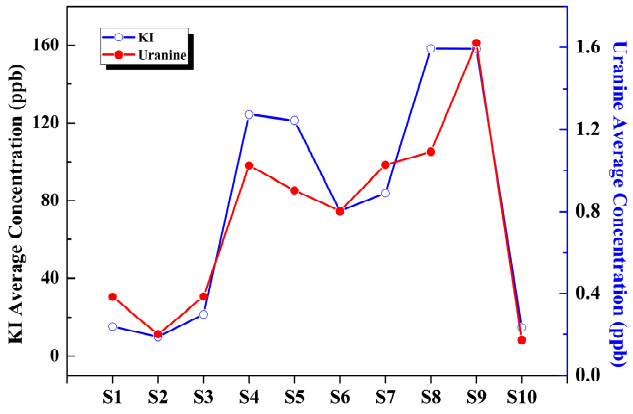

Figure 3. The average concentration of two tracers for each receiving point.

Due to the great difference in the amount of two tracers which were injected in Jiuzi Sea, two kinds of tracer concentrations in the same spring can show profound discrepancy. The double Y axis of two kinds of tracers with large difference in the concentration values show the same characteristics, when we adjust the numerical range of two Y axes reasonably. In Figure 3, the average concentration of the tracer in S1–S3 and S10 are lower than those of any other springs located in the south area to topography watershed.

4. Discussion

4.1. Hydraulic Connection between the Jiuzi Sea and Receiving Springs

According to those curves in Figure 2, both tracers can be detected at each receiving spring, which confirms the hydraulic connection between the Jiuzi Sea and ten downstream springs. This means that the complex karst conduit connects the recharge water in this giant sinkhole to both southern and northern groundwater systems on both sides of the topography watershed.

In general, broken rocks of fault in karst formations have good permeability. Some researchers consider that karst conduits can form more easily in this area [13,36,37]. The high topography northern to the Jiuzi Sea cannot prevent the recharge water from going northward, which might be attributed to that the F_2 goes through the topography watershed. Some conduit develops in the broken rocks of F_2 from Jiuzi Sea to northern area to topography watershed, where the main aquifer compose of the strata of T_2b^3 and T_2b^2 appears. Hence, the northern flow path in this study area probably develops along F_2 firstly, then passes through in the aquifer compose of the strata of T_2b^3 and T_2b^2, and ends near the aquifer boundary where S10 appears (Figure 1C). Based on the tracer connection in this test, the assumed karst conduit network of the study area is illustrated in Figure 4A, which describes one injection point and the divergent flow. However, this figure only shows the conduit connection and the specific conduit location cannot be determined.

4.2. Structure of the Karst Conduits System

4.2.1. Injection Conditions and Discharge Variation Effects in BTCs

Many reasons for multi-peaks, injection conditions and discharge variation during the test should be considered. Maurice et al. made two injections in the same point to study the karstic behaviors of groundwater in the English Chalk [14]. It was found that the concentration returned to background level between two peaks, and that the interval of these two peaks was almost equal to that of those two injections. Morales et al. conducted a long-term tracer injection, and they discovered that the concentration returned to the background level several times to form multi-peaks in the BTC [38]. Both staged injections and long-term tracer injections similar to staged injections can produce multi-peaks, but the BTCs correspond to a single conduit. In our test, the tracers were injected into a sinkhole within 2 h, and enough water was injected to make tracers go under the groundwater. During the test period, there was no rainfall and the discharge was almost constant (Figure 2). Hence, the interval of multi-peaks in our test should not be caused by the staged injection and long-term tracer injection, but should be caused by multi-conduits.

Thus, in the BTCs of our test, the multi-peaks with relatively long interval should correspond to multi-conduits, such as S1, S2, S3, S4 and S10. Each major peak of these springs shows the characteristics of tailing phenomenon and symmetric upper half, which are usually observed in conduit-dominated karst aquifer [5,26,39]. Numerous experiments have reported that the shape of the tracer concentration versus time plot has strong correlation with the karst conduit structure [4,9,10]. Some previous conclusions are as follows:

- The unimodal curve with large kurtosis corresponds to a single karst conduit.
- The unimodal curve with gradual descending trend or steps on the falling limb corresponds to a single karst conduit with a reservoir (or reservoirs).
- The unimodal curve with many independent or continuous slight peaks corresponds to karst conduits with some fractures.

According to the above arguments, the injection conditions and discharge variation effect in BTCs, Table 4 shows the karst conduit structure corresponding to every spring, and their characteristics are discussed as follows.

4.2.2. Conduit Characteristics of Receiving Springs

The conduit structure according to the BTCs are shown in Table 6. Based on the number of unimodal curves, the conduit of springs are divided into two kinds: multiple conduits and single conduit.

1. Multiple conduits (S1, S2, S3, S4 and S10)

Multi-peaked curves suggest the presence of bifurcated flow paths, and the peaks with a considerable distance indicate the great differences in the length and permeability of various paths [4,7,9,40]. Springs (S1, S2 and S3) in Black Dragon Pool appear very closely, so the corresponding three curves are uniformly distributed in the form of intermittent pulses with obviously separated major peaks. This indicates that there should be three main conduits with different distances and permeabilities.

The BTCs of $II_{1–3}$ and II_{10} show the characteristics of baseline concentration, long resident time and slow descending, indicating that the main conduit is probably a big karst space such as a reservoir [7,9,10]. Some researchers considered that the slight peaks resulted from proximal mixing of tracer water with the dilution [4] However, there was no rainfall and the flow rate was almost constant during the test period (as shown in Figure 2A–C). This means that proximal mixing cannot occur during our test without additional discharge water. On the other hand, fractures usually carry less amount of tracer than karst conduits due to their limited length, which can lead to the slight peaks on the curves. Consequently, the slight and concentrated peaks observed during the peak pulse of $III_{1–3}$ can be viewed as the characteristics of conduits-dominated and fissures-assisted flow [10].

Figure 2D corresponding to S4 indicates that two major karst conduits exist between the Jiuzi Sea and S4, i.e., I_4 and II_4 (Table 4). It is worth mentioning that steps can be found on falling limbs in I_4 section of the two curves, which almost have identical unanimity with time. The shape of the curves just reflects the specific performance of underground conduits with relatively large size [11,40,41].

2. Single conduit (S5, S6, S7, S8, and S9)

According to Figure 2E–I, the unique strong peak positively confirms that only one major karst conduit exists between the Jiuzi Sea and each spring. The relatively short resident time for the low flux indicates the small scale of the corresponding conduit, and the low flux also indicates the little turbulent flow. Both can cause more viscous sublayer [5,42]. Thus, the low flux and the weak tailing phenomenon of these curves may reveal the weak pseudo-laminar flow near to the conduit wall, and confirm the small scale of the conduit.

The strong concentration fluctuation of major peaks appears, for example, in BTCs of S7. To understand this phenomenon, the high heterogeneity of the karst subterraneous system inspires us to consider the storage zones along the tracer path. These storage zones can be deemed as immobile zones of the karst conduit branch or occasionally connected fractures [13], and more tracer can deposit in the immobile zones based on the small flux situation and the hypothesis of small-scale conduit. In our test, the flow velocity could reach about 1 km/day and the tracer recovery rate was very low (Table 5). Relatively rapid flow and low tracer recovery indicate the high storage percentage in the karst. Some researchers conjectured that there was limited connected conduit network in the paths where the tracers passed [1,15,22].

4.3. Tracer Velocity and Recovery

In highly karstified aquifers, the flow velocity can be up to several kilometers per day, which is the character of turbulent conduit flow. In the Mendip Hills, Great Britain, the mean flow velocity is 6.33 km/day [22]. In the classical karst area on the border between Slovenia and Italy, the apparent maximum tracer velocity is 1.83 km/day [24]. In the Xiangxi River Basin of southern China, the flow velocity can reach 5.76 km/day in August [43]. In our test, the tracer velocity ranges from 0.80 to 2.30 km/day (Table 3). By contrast, in the mildly karstified aquifer in Chalk, the tracer velocity can reach 5 km/day, which is as rapid as that of the highly karstic aquifers. Maurice considered that this conduit in Chalk had many fissures and voids with limited connectivity [15].

Table 4. Peak times and C(t)/Cp at peak times for every receiving point.

Spring No.	Location	The Name of Receiving Springs	KI			Uranine		
			Peak Times (h)	$C(t)/C_p$ at Peak Times	Tracer Velocity * (10^{-2}m/s)	Peak Times (h)	$C(t)/C_p$ at Peak Times	Tracer Velocity * (10^{-2}m/s)
S1	Black Dragon Pool	Longevity spring	222 h, 310 h, 432 h	0.34, 0.61, 1.00	2.05, 1.47, 1.05	204 h, 308 h, 420 h	0.22, 0.52, 1.00	2.23, 1.47, 1.08
S2		Pearl spring	220 h, 304 h, 419 h	0.56, 0.94, 1.00	2.07, 1.50, 1.09	198 h, 292 h, 412 h	0.14, 0.68, 1.00	2.30, 1.56, 1.11
S3		Gate spring	218 h, 290 h, 448 h	0.50, 0.59, 1.00	2.09, 1.57, 1.02	224 h, 284 h, 414 h	0.68, 1.00, 0.68	2.03, 1.60, 1.10
S4	Clear Reservoir	Clear spring	198 h, 276 h	0.65, 1.00	2.19, 1.57	198 h, 294 h	0.91, 1.00	2.19, 1.47
S5	Ancient city	White horse Pool spring	262 h	1.00	1.72	258 h	1.00	1.74
S6		Three eyes Well spring	306 h	1.00	1.47	282 h	1.00	1.63
S7		Sweet spring	266 h	1.00	1.60	270 h	1.00	1.63
S8	Along the F_1	Lotuses spring	198 h	1.00	1.81	188 h	1.00	1.90
S9		Rock spring	198 h	1.00	1.32	180 h	1.00	1.45
S10	White river	White spray spring	484 h, 568 h	1.00, 0.63	0.96, 0.82	472 h, 584 h	1.00, 0.76	0.98, 0.80

* Tracer velocity is calculated by the equation: $v = s/$, where v is the linear tracer velocity, s is the direct distant from the injection point to the receiving springs, and t is the peak time.

Table 5. Tracer recovery rate (%) for every receiving springs.

Tracers	Tracers Recovery of Receiving Springs										Total
	S1	S2	S3	S4	S5	S6	S7	S8	S9	S10	
KI (×100)	0.01	0.31	0.12	5.92	0.17	0.51	0.51	0.48	0.10	4.82	13.68
Uranine (×100)	0.02	0.87	0.32	5.59	0.30	0.61	0.72	0.08	0.15	6.21	15.62

Table 6. Spatial characterizations of the karst conduits for every receiving spring.

	S_1 (Springs in Black Dragon Pool)			**S_2 (Pearl Spring)**			**S_3 (Gate Spring)**			**S_4 (Clear Spring)**		**S_5 (White Horse Pool Spring)**
Major karst channels	I_1	II_1	III_1	I_2	II_2	III_2	I_3	III_3	III_3	I_4	II_4	I_5
Fracture development	+			+			+					+
Numbers of pool		1			1			1				
	S_6 (Three Eyes Wells)			**S_7 (Sweet Spring)**			**S_8 (Lotuses Spring)**			**S_9 (Rock Spring)**		**S_{10} (White Spray Spring)**
Major karst channels	I_6			I_7			I_8			I_9		I_{10} I_{10}
Fracture development												
Numbers of pool												1 1
The karst conduit for every springs	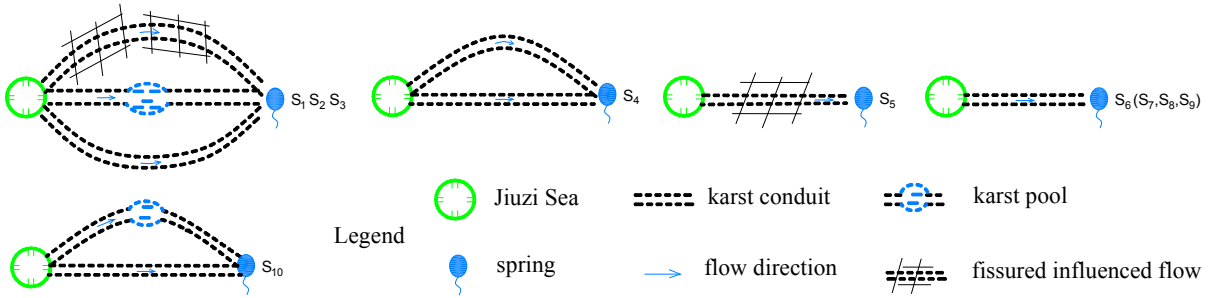											

* "+" refers to "positive" in fracture development.

S1, S2, and S3 have different flow velocities. The rapid flow in I_{1-3} is obvious conduit flow and the slow flow in III_{1-3} has conduits-dominated and fissures-assisted characteristics. The dual-permeability phenomenon (conduits and fissures) can result in strong tailing, and the decrease of flow velocity can increase the tracer sedimentation [5,41]. This may be used to explain the stronger tailing effects and lower tracer velocity of III_{1-3} than those of I_{1-3}. The conduit corresponding to II_{1-3} also has strong tailing, and the resident time is the longest. This indicates that the conduit is of large scale, which can decrease the flow velocity and increase the dilution effects. The peak of II_{10} is similar. Comparatively, the springs in the Ancient City and F_1 (S5, S6, S7, S8, and S9) have lower velocities than the first velocity in I_{1-3} (Table 4), which can produce more viscous sublayer in smaller conduits.

In highly karstified areas, the attenuation of tracer recovery is low. Atkinson considered that the conduit flow accounted for most water transmission in the aquifer, with the tracer recovery ranging from 60% to 80% [23]. In the Noville aquifer system, France, four tracer tests were conducted, and the tracer recovery ranged from 88.2% to 95.4% [5]. Several tracer tests were also carried out in the Xiangxi River Basin of southern China, and the maximum tracer recovery was 64%. By contrast, in mildly karstified areas, even if the flow velocity reached several kilometers per day, the tracer recovery was only 25–35% [15]. Maurice considered that the significant attenuation was probably due to the dispersion of tracers from the main conduit flow paths into small voids [15]. In our test, although the study area is a well-developed karst system, the flow velocity is relatively lower compared to that of other karst areas discussed above. Thus, there are probably a large number of voids with limited connection similar to those in Chalk. This is one main reason for the low tracer recovery in our test (Table 6), and the attenuation of tracer recovery induced by this may be stronger in the long-distance tracer test. In the dry season, tracers can deposit more readily in small pores because of the low flux, so the attenuation may become more significant [5]. Hence, in this study, the relatively low flux in the dry season can also strengthen the low recovery. For S1, S2, and S3, the characteristics of their BTCs (Figure 3), such as the lowest concentration of all springs located south to Jiuzi Sea, also similar to S10, obvious tailing phenomenon and relatively long resident time, generally correspond to a conduit with an underground reservoir, and the strong tracer dilution in the reservoir may be another reason for the low tracer recovery.

4.4. Conceptual Conduit Structure for Springs (S1–S3 and S5–S7)

S1–S3 are the main water source for the Ancient City of Lijiang. According to the above arguments, the main conduit connecting with Black Dragon Pool is considered as a reservoir. This may be the main reason for the low tracer recovery and low tracer concentration. Furthermore, the large flow rate in history also confirms the existence of large-scale flow path. In our test, most of the tracer was stored in the reservoir, and might discharge in a very long period with a very low concentration beyond the detection limit. Meanwhile, the springs in the Ancient City near to Black Dragon Pool have never dried up, and their flux kept constant in history with lower altitudes than the springs in Black Dragon Pool. According to the distribution of these springs and considering the same main source, a conceptual conduit structure of a leaky reservoir with threshold effect above a certain groundwater level was proposed [44]. As shown in Figure 4C, the springs in Black Dragon Pool (S1, S2, and S3) and the Ancient City (S5, S6, and S7) are assumed as the thresholds gap and leaks, respectively. Only when the water level in the karst aquifer is higher than the blue line in Figure 4C, there will be a flow discharging from Black Dragon Pool, and the groundwater can dilute the concentration of the tracers from the conduit. Meanwhile, S5, S6, and S7 are the leaks in the karst aquifer. When the water level in the karst aquifer is between the red line and the blue line, as shown in Figure 4C, the springs in Black Dragon Pool dry up but those in the Ancient City remain flow.

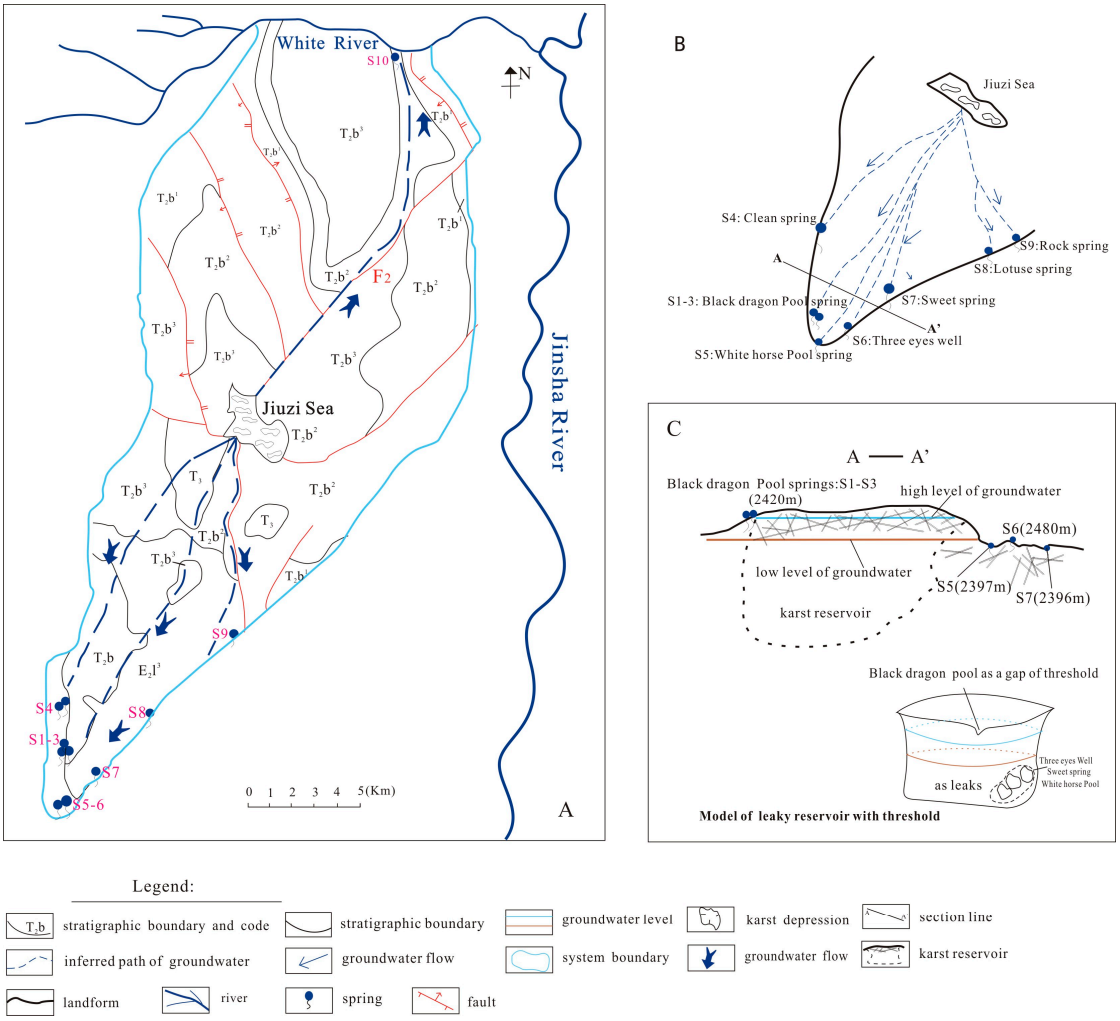

Figure 4. The distribution sketch of inferring karst conduits and conceptual conduit structure of springs in the Black Dragon Pool: (**A**) the proven hydraulic connection by BTCs of our trace test; (**B**) the conduits distribution from the Jiuzi Sea to southern springs, and the profile line of A-A'; and (**C**) the profile of A-A' and a leaky reservoir with threshold effect which is used to interpret the conceptual conduit structure of springs in Black Dragon Pool and Ancient City.

Meanwhile, S4 S8 and S9 are located in the west and east part to the Black Dragon Pool and are further from it than springs in Ancient City. They have never dried up, although they appear higher than springs in Black Dragon Pool. It shows that they have no uniform groundwater level as the springs in Black Dragon Pool, and their conduits are independent of them, as the supposed conduits connection shown in Figure 4A,B.

5. Conclusions

In summary, our tracer test indicates that the recharge water in the giant depression of the Jiuzi Sea is one main source for all receiving springs, and that the complex karst conduits connect the recharge water with both southern and northern groundwater systems on both sides of the topography watershed. The groundwater system has divergent flow to multiple outlets. The southwestern springs (S1, S2, S3 and S4) have multi-conduits, while the southeastern springs (S5, S6, S7, S8 and S9) have a single conduit. The more intensive conduits in the western zone indicate the stronger karst development degree, which is consistent with the large-scale conduit in Black Dragon Pool.

The tracer velocity ranging from 0.80 to 2.30 km/day in our test is comparable to that in many highly karstified aquifers, and the first velocity in southwestern area is quicker than that in southeastern area. The tracer recovery is very low, as long-distance flow paths with complex karstic structure can cause strong attenuation of tracer recovery. Thus, the ratio of limited connection voids in the study area is relatively higher than that in highly karstified areas. The randomness is considered as the main reason for the different trace properties of KI and uranine according to the long-distance flow path and complex structure. Due to the utilization of I^- by organism, the tracer recovery of KI is a little lower than that of Rose Bengal.

Based on the BTCs and tracer velocities, it can be concluded that the area in Black dragon Pool is highly karstified with complex conduit network. The tracer dilution in big conduits such as reservoirs can also lead to the lower tracer recovery, which corresponds to the very low concentration and the BTCs of II_{1-3} with strong tailing, long resident time and steps on falling limbs. Furthermore, the springs (S1, S2, and S3) with higher height have dried up several times while the springs (S5, S6, and S7) in the Ancient City have never in history. A conceptual conduit structure of leaky reservoir with threshold effect above a certain groundwater level is adopted to interpret this phenomenon. The groundwater can flow out through the gap of the threshold only if it fills up the reservoir, while it springs in the Ancient City as leaks never cut off. This means that the dried springs can probably recover by injecting nearby river water into the Jiuzi Sea. Hydraulic connection shows that not the topography of the watershed but the complex karst conduit in this study area control the groundwater flow; the key problem to recover the water source is to limit the increased recharge from the river flowing northward.

Author Contributions: Conceptualization, Q.J.H.; Methodology, X.M.; Investigation, Z.Q.; Data Curation, C.X.Y. and W.L.

Funding: This work is partially supported by the Natural Science Foundation of China (Grant No. 41402223).

Acknowledgments: The authors also appreciate the aid for improvements of the paper from Water Resources and Hydropower Survey and Design Institute, Lijiang.

Conflicts of Interest: The authors declare no conflict of interest.

References

1. Ford, D.C.; Williams, P.W. Karst Geomorphology and Hydrology. *J. Geol.* **1991**, *98*, 797–798.
2. Werner, K. *Tracer Technique in Geohydrology*; Balkama: Rotterdam, The Netherlands, 1998; pp. 581–583.
3. Goldscheider, N.; Drew, D. *Method in Karst Hydrogeology*; Taylor and Francis: Oxford, UK, 2007; p. 264.
4. Smart, C.C. Artificial tracer techniques for the determination of the structure of conduit aquifers. *Groundwater* **1988**, *26*, 445–453. [CrossRef]
5. Massei, N.; Wang, H.Q.; Field, M.S.; Dupont, J.P.; Bakalowicz, M.; Rodet, J. Interpreting tracer breakthrough tailing in a conduit-dominated karstic aquifer. *Hydrogeol. J.* **2006**, *14*, 849–858. [CrossRef]
6. He, S.Y.; Michele, L.; Zhang, C.A. High Precision Underground Water Tracing Test Technique and Its Applications: A Case Study in Maocun Karst System, Guilin, Guanxi. *Acta Geosci. Sin.* **2009**, *30*, 673–678, (In Chinese with English Abstract).
7. Field, M.S.; Leij, F.J. Solute transport in solution conduits exhibiting multi-peaked breakthrough curves. *J. Hydrol.* **2012**, *440*, 26–35. [CrossRef]
8. Goldscheider, N. Overview of Methods Applied in Karst Hydrogeology. In *Karst Aquifers—Characterization and Engineering*; Springer International Publishing: New York, NY, USA, 2015; pp. 127–145.
9. Yang, L.Z.; Liu, J.Y. Structure-time curve of tracer concentration test analysis of karst pipe. *J. Chengdu Univ. Technol.* **1979**, *4*, 211–219, (In Chinese with English Abstract).
10. Zhang, Z.W. Types of conduit flow field of karstic groundwater versus tracer curves and their practical application. *Carsol. Sin.* **1990**, *9*, 211–219, (In Chinese with English Abstract).
11. Zhang, Z.W.; Zou, C.J. Principle of tracing and detecting karst groundwater dispersive flow field and application in reservoir leakage study. *Carsol. Sin.* **1995**, *14*, 252–260, (In Chinese with English Abstract).

12. Smart, C.C.; Ford, D.C. Structure and function of a conduit aquifer. *Can. J. Earth Sci.* **1986**, *23*, 919–929. [CrossRef]
13. Kübeck, C.; Maloszewski, P.J.; Benischke, R. Determination of the conduit structure in a karst aquifer based on tracer data-Lurbach system, Austria. *Hydrol. Process.* **2013**, *27*, 225–235. [CrossRef]
14. Maurice, L.D.; Atkinson, T.C.; Barker, J.A. Karstic behavior of groundwater in the English Chalk. *J. Hydrol.* **2006**, *330*, 63–70. [CrossRef]
15. Maurice, L.D.; Atkinson, T.C.; Barker, J.A.; Williams, A.T.; Farrant, A.; Gallagher, A. Tracer investigation of nature and structure of subsurface voids in mildly karstic aquifers: An Example from the English chalk. In *Advances in Research in Karst Media*; Springer International Publishing: New York, NY, USA, 2010; pp. 137–142.
16. Wang, Y. Study on exploitation and utilization condition of karst groundwater in Yunan Province. *J. Hydraul. Eng.* **2001**, *32*, 49–52, (in Chinese with English abstract).
17. Fan, T.; Yang, S.Y. Groundwater vulnerability assessment in Lijiang Basin. *J. Jilin Univ.* **2007**, *37*, 551–556, (In Chinese with English abstract).
18. Kang, X.B.; Wang, Y.; Zhang, H.; Cao, J. Hydro-geologic features and influence factors of zero flow of the Heilongtan spring group in Liiang. *Carsol. Sin.* **2013**, *32*, 398–402, (in Chinese with English abstract).
19. Geyer, T.; Birk, S.; Licha, T. Multitracer Test Approach to Characterize Reactive Transport in Karst Aquifers. *Groundwater* **2007**, *45*, 36–45. [CrossRef] [PubMed]
20. Smart, P.L.; Smith, D.I. Water tracing in tropical regions, the use of fluorometric techniques in Jamaica. *J. Hydrol.* **1976**, *30*, 179–195. [CrossRef]
21. Davis, S.N.; Thompson, G.M.; Bentley, H.W.; Stiles, G. Ground-water tracers—A short review. *Groundwater* **1980**, *18*, 14–23. [CrossRef]
22. Anderson, D.H.; Eisenfeld, J.; Saffer, S.I. The mathematical analysis of four-compartment stochastic model of rose-bengal transport through the hepatic system. In *Nonlinear Systems and Applications*; Lakshmikantham, V., Ed.; Academic Press: Cambridge, MA, USA, 1977; pp. 353–371.
23. Sabatini, A.D. Sorption and intraparticle diffusion of fluorescent dyes with consolidated aquifer media. *Groundwater* **2000**, *38*, 651–656. [CrossRef]
24. Petrič, M.; Kogovsek, J. Identifying the characteristics of groundwater flow in the Classical Karst area (Slovenia/Italy) by means of tracer test. *Environ. Earth Sci.* **2016**, *75*, 1446–1459. [CrossRef]
25. Field, M.S. A review of some tracer-test design equations for tracer-mass estimation and sample-collection frequency. *Environ. Geol.* **2002**, *43*, 867–881. [CrossRef]
26. Worthington, S.R.H.; Smart, C.C. Empirical equations for determining tracer mass for sink to spring tracer testing in karst. In *Sinkholes and the Engineering and Environmental Impacts of Karst*; Bech, B.F., Ed.; American Society of Civil Engineers: Reston, VA, USA, 2003; pp. 287–295.
27. Xue, Y.Q.; Wu, J.C. *Groundwater Hydraulics*, 2nd ed.; Geological Publishing House: Beijing, China, 2010; pp. 14–15.
28. Yang, Q.K. Discussion on the uncertainty of ground water resource in karst area of Guilin. *Carsol. Sin.* **1985**, *1*, 58–62, (In Chinese with English abstract).
29. Yi, L.X.; Xia, R.Y.; Wang, Z. Infiltration coefficient of precipitation in karst peak-cluster depression area: A case study of Zhaidi karst underground river basin. *Carsol. Sin.* **2017**, *36*, 512–517.
30. Kilpatrick, F.A.; Wilson, J.F., Jr. Measurement of time of travel in streams by dye tracing. In *Techniques of Water-Resources Investigations of the US Geological Survey*; USGS: Reston, VA, USA, 1989; pp. 13–25.
31. Hauns, P.M.; Jeannin, Y.; Atteia, O. Dispersion, retardation and scale effect in tracer breakthrough curves in karst conduits. *J. Hydrol.* **2001**, *241*, 177–193. [CrossRef]
32. Reimus, P.W.; Arnold, B.W. Evaluation of multiple tracer methods to estimate low groundwater flow velocities. *J. Contam. Hydrol.* **2017**, *199*, 1–13. [CrossRef] [PubMed]
33. James, G.; Witten, D.; Hastie, T.; Tibshirani, R. *An Introduction to Statistical Learning*; Springer International Publishing: New York, NY, USA, 2017; pp. 31–32.
34. Murray, K.E.; Straud, D.R.; Hammond, W.W. Characterizing groundwater flow in a faulted karst system using optical brighteners from septic systems as tracers. *Environ. Geol.* **2007**, *53*, 769–776. [CrossRef]
35. Cui, L.Y.; Huang, J.J.; Wu, X.; Chen, J.H.; Jiang, G.Q.; Xu, S.Y. The control of the formation of karst collapse through the ancient Yellow River Fault zone in Xuzhou, China. *Carbonates Evaporites* **2017**. [CrossRef]

36. Abdullah, D.; Fayez, A.; Nizar, H.; Mutewekil, O. Karst development related to extensional fracture network at Bany-Kanana area, northern Jordan. *Arab J. Geosci.* **2015**, *8*, 4999–5014.
37. Morales, T.; Angulo, B.; Uriarte, J.A. Solute transport characterization in karst aquifers by tracer injection tests for a sustainable water resource management. *J. Hydrol.* **2017**, *547*, 269–279. [CrossRef]
38. Goldscheider, N.; Meiman, J.; Pronk, M. Tracer tests in karst hydrogeology and speleology. *Int. J. Speleol.* **2008**, *37*, 27–40. [CrossRef]
39. Lorraine, D.; Isabelle, B.; Gaetan, R.; Vincent, H. Solute transport in heteogeneous karst system: Dimensioning and estimation of transport parameters via mult-sampling tracer-tests modelling using the OTIS (One-dimensional Transport with inflow and Storage) Program. *J. Hydrol.* **2016**, *534*, 567–578.
40. Tomas, M.; Fuez, L.; Valderrama, D.; Jesus, A.U.; Inaki, A.; Martin, O. Predicting travel times and transport characterization in karst conduit by analyzing tracer-breakthrough curves. *J. Hydrol.* **2007**, *334*, 183–198.
41. Maloszewski, P.; Zuber, A.; Bedbur, E.; Matthess, G. Transport of three herbicides in ground water at Twin Lake test site, Chalk River, Ontario, Canada. *Groundwater* **2003**, *41*, 376–386. [CrossRef]
42. Atkinson, T.C. Diffuse flow and conduit flow in limestone terrain in the Mendip Hills, Somerset (Great Britain). *J. Hydrol.* **1977**, *35*, 93–110. [CrossRef]
43. Luo, M.; Chen, Z.; Zhou, H.; Jakada, H.; Zhang, L.; Han, Z.; Shi, T. Identifying structure and function of karst aquifer system using multiple field methods in karst trough valley area, South China. *Environ. Earth Sci.* **2016**, *75*, 1–13. [CrossRef]
44. Ke, K.; Zhu, L.M.; Li, Z. *Hydraulics*; Science Press: Beijing, China, 2003. (In Chinese)